Reactions of Nitric Oxide with the Reduced Non-Heme Diiron Center of the Soluble Methane Monooxygenase Hydroxylase†

David E. Coufal,‡ Pedro Tavares,§ Alice S. Pereira,§ Boi Hanh Hyunh,|| and Stephen J. Lippard*,‡

Department of Chemistry, Massachusetts Institute of Technology, Cambridge, Massachusetts 02139, Department of Chemistry, Universidade Nova de Lisboa, Lisbon, Portugal, and Department of Physics, Emory University, Atlanta, Georgia 30322

Received September 29, 1998

ABSTRACT: The soluble methane monooxygenase system from *Methylococcus capsulatus* (Bath) catalyzes the oxidation of methane to methanol and water utilizing dioxygen at a non-heme, carboxylate-bridged diiron center housed in the hydroxylase (H) component. To probe the nature of the reductive activation of dioxygen in this system, reactions of an analogous molecule, nitric oxide, with the diiron(II) form of the enzyme (H_{red}) were investigated by both continuous and discontinuous kinetics methodologies using optical, EPR, and Mössbauer spectroscopy. Reaction of NO with H_{red} affords a dinitrosyl species, designated $H_{dinitrosyl}$, with optical spectra (λ_{max} = 450 and 620 nm) and Mössbauer parameters (δ = 0.72 mm/s, ΔE_Q = 1.55 mm/s) similar to those of synthetic dinitrosyl analogues and of the dinitrosyl adduct of the reduced ribonucleotide reductase R2 (RNR-R2) protein. The $H_{dinitrosyl}$ species models features of the H_{peroxo} intermediate formed in the analogous dioxygen reaction. In the presence of protein B, $H_{dinitrosyl}$ builds up with approximately the same rate constant as H_{peroxo} ($\sim$26 s^{-1}) at 4 °C. In the absence of protein B, the kinetics of $H_{dinitrosyl}$ formation were best fit with a biphasic A → B → C model, indicating the presence of an intermediate species between H_{red} and $H_{dinitrosyl}$. This result contrasts with the reaction of H_{red} with dioxygen, in which the H_{peroxo} intermediate forms in measurable quantities only in the presence of protein B. These findings suggest that protein B may alter the positioning but not the availability of coordination sites on iron for exogenous ligand binding and reactivity.

The soluble methane monooxygenase (sMMO)[1] enzyme system in methanotrophic bacteria catalyzes the oxidation of methane to methanol and water by using dioxygen as an oxidant at a non-heme carboxylate-bridged diiron center (*1*−*5*). One atom of the dioxygen molecule is incorporated into the product alcohol, and the other is released as water. Two electrons from NADH and two protons are also required. The controlled oxidation of hydrocarbons by this and similar systems is a topic of considerable current interest.

The sMMO system has three known protein components. The hydroxylase (H) is a homodimer ($\alpha_2\beta_2\gamma_2$) that contains a non-heme diiron center in each of its α subunits. The iron center is the locus of dioxygen activation and methane hydroxylation. The reductase (R) is responsible for transferring electrons from NADH through protein-bound FAD and [2Fe-2S] centers to the diiron center in the hydroxylase. A third component, protein B or the coupling protein, serves to couple this electron transfer to alkane hydroxylation.

The catalytic cycle of the hydroxylase enzyme has been examined in detail by using a variety of rapid kinetics methodologies, including optical stopped-flow and freeze-quench Mössbauer spectroscopy. Typically, the iron center is chemically reduced to the diiron(II) state, designated H_{red}, and mixed rapidly with solutions containing dioxygen. The first well-characterized intermediate after H_{red} is H_{peroxo} (*6*, *7*), assigned as a (μ-1,2-peroxo)diiron(III) species through spectroscopic comparison with crystallographically characterized model compounds (*8*−*10*). The H_{peroxo} intermediate spontaneously transforms into intermediate Q (*6*, *7*), which has been assigned a di(μ-oxo)diiron(IV) structure on the basis of EXAFS evidence (*11*), although other interpretations of the data are possible (*1*). Intermediate Q reacts with alkane substrates to form hydroxylated products, returning the catalytic center to its resting, diiron(III) state, designated H_{ox}.

The role of protein B is not well understood. The cycle described above does not take place if protein B is absent. The diiron(II) center is instead oxidized to the diiron(III) state without observable accumulation of the H_{peroxo} and Q intermediates. Under steady-state conditions, protein B from the *Methylococcus capsulatus* (Bath) sMMO system has a dramatic effect on turnover (*12*, *13*). When it is not present, hydroxylation of products is completely uncoupled from dioxygen and NADH consumption. Instead, dioxygen is reduced to water. As protein B is added to the system, the

† This work was supported by grants from the National Institute of General Medical Sciences (GM32134 to S.J.L. and GM47295 to B.H.H.). P.T. and A.S.P. were supported by postdoctoral research fellowships from Programa PRAXIS XXI of Junta Nacional de Investigaco Cientifica e Tecnologica, Portugal. D.E.C. was a Predoctoral Fellow of the National Science Foundation.

* To whom correspondence should be addressed.
‡ Massachusetts Institute of Technology.
§ Universidade Nova de Lisboa.
|| Emory University.

[1] Abbreviations: sMMO, soluble methane monooxygenase; H_{ox}, diiron(III) sMMO hydroxylase; H_{red}, diiron(II) sMMO hydroxylase; H_{peroxo}, diiron(III) peroxo intermediate form of the sMMO hydroxylase; $H_{dinitrosyl}$, dinitrosyl adduct of H_{red}; RNR-R2, ribonucleotide reductase R2 subunit; MOPS, 3-(*N*-morpholino)propanesulfonic acid; RFQ, rapid freeze-quench.

10.1021/bi9823378 CCC: $18.00
Published on Web 03/16/1999

Table 1: Spectroscopic Properties of Non-Heme Carboxylate-Bridged Diiron Dinitrosyl Complexes

sample	optical properties λ_{max} (nm) [ϵ (M^{-1} cm^{-1})]	Mössbauer properties δ (mm/s)	Mössbauer properties ΔE_Q (mm/s)	ref
$[Fe_2(NO)_2(Et\text{-}HPTB)(OBz)]^{2+}$	520 (395), 620 (579)	0.67	1.44	*48*
E. coli ribonucleotide reductase R2 (dinitrosyl)	450 (760), 620 (220)	0.75	−2.13, −1.73	*26*
P. gouldii hemerythrin (mononitrosyl)	408 (1200), 500 (700), 600 (500)	0.68, 1.21 Fe(II)	0.61, 2.65 Fe(II)	*24*, *15*
dinitrosyl adduct of $[Fe_2(\mu\text{-XDK})(\mu\text{-}O_2CPh)(ImH)_2(O_2CPh)(MeOH)]$	450 (2100), 630 (670)	0.74	1.41	*33*

extent of coupling of hydroxylated product formation to dioxygen consumption increases. At a 1:1 ratio of protein B to hydroxylase, the system is fully coupled. As the ratio of protein B to hydroxylase increases beyond 1, the hydroxylation reaction is inhibited. These observations are consistent with protein B having a role as a regulatory protein. The coupling protein also has a direct effect on the iron center. The presence of protein B causes the $g = 16$ integer spin EPR signal of H_{red} from *Methylococcus trichosporium* OB3b to become sharper and more intense (*14*). Magnetic circular dichroism experiments indicate that protein B effects a major coordination change at one of the iron atoms in the active site (*15*, *16*), the details of which are obscure. Knowledge of these changes is crucial both for structurally modeling and for comprehending the mechanism of the sMMO system.

Nitric oxide is a surrogate for dioxygen (*17*) and reacts similarly with iron to afford complexes having useful spectroscopic properties. Species produced by the reaction of iron(II) with nitric oxide typically are brightly colored, $S = {}^3/_2$ systems (*18*−*20*) with characteristic EPR signals (*21*−*23*), and are designated as $\{Fe(NO)\}^7$ (*20*), where the superscript refers to the sum of d electrons from iron and π^* electrons from the NO molecule.

Nitric oxide has been useful as a probe of non-heme, carboxylate-bridged diiron centers. In hemerythrin (Hr), one NO molecule binds to a single iron atom (*24*, *25*). The resulting $\{Fe(NO)\}^7$ center couples antiferromagnetically with the other high-spin iron(II) center to form an EPR-active, $S = {}^1/_2$ spin system. The mode of NO binding was proposed to be very similar to that of O_2, with the uncoordinated oxygen atom of the NO ligand forming a hydrogen bond with the hydroxide bridge present in deoxyhemerythrin. This proposal was supported by a shift in the Raman spectrum due to changes in the Fe−N−O bending mode upon deuteration of the bridge. In the R2 subunit of ribonucleotide reductase, a more complex, heterogeneous reaction was observed (*26*). Addition of NO to the diiron(II) center of this protein afforded a complex having optical features at 450 and 620 nm. Mössbauer spectra of the product revealed a mixture with the following composition: 77% diiron dinitrosyl species $[\{Fe(NO)\}^7]_2$, 13% mononuclear $\{Fe(NO)\}^7$, and 10% unidentified species. The two $S = {}^3/_2$ $\{Fe(NO)\}^7$ centers in the diiron dinitrosyl adduct were antiferromagnetically coupled to form an EPR-silent species, which decomposed with first-order kinetics, reductively coupling the two NO molecules to form N_2O and oxidized RNR-R2. This diiron dinitrosyl species was proposed to be a model of the peroxo intermediate in the RNR-R2 reaction cycle. The spectroscopic properties of these and selected model compounds with carboxylate-bridged, non-heme diiron centers complexed with NO are listed in Table 1.

This article describes a study of the reactions of NO with the reduced diiron center of the sMMO hydroxylase from *M. capsulatus* (Bath). These experiments afford the opportunity not only to model the O_2 binding step but also to probe the role of protein B. The results provide new information about how the coupling protein can alter the dinuclear iron center for reaction with dioxygen.

EXPERIMENTAL PROCEDURES

Preparation and Purification of sMMO Hydroxylase (H) and Protein B. Samples of sMMO hydroxylase and of ^{57}Fe-enriched sMMO hydroxylase were prepared from *M. capsulatus* (Bath) as previously described (*27*). Protein B was prepared from a cloned source in *Escherichia coli* as reported previously (*28*). The purity of the components was assured by SDS−PAGE. The specific activity and iron content were measured as described and were in the range of 250−350 nmol of propylene oxide formed mg^{-1} min^{-1} and 3.4−3.7 Fe/protein, respectively.

Preparation of Diiron(II) sMMO Hydroxylase (H_{red}). Purified sMMOH samples were prepared in 25 mM MOPS (pH 7.0) with stoichiometric amounts of the mediator methyl viologen. The sample was degassed by 15−20 cycles of vacuum evacuation followed by argon backfilling. A degassed solution of ∼10 mM sodium dithionite in 50 mM MOPS (pH 8.6) buffer was prepared and used to titrate the protein solution until the methyl viologen changed from yellow to blue. A 30 min time period was sufficient for complete reduction. The sample was then anaerobically dialyzed against two successive 500 mL volumes of 25 mM MOPS (pH 7.0) to remove the mediator and reductant.

Addition of NO Gas. H_{red} samples were prepared and placed in vials sealed with rubber septa both with and without 2 equiv of protein B. Nitric oxide (>99%, Matheson) was purified by passage through a concentrated NaOH solution to remove NO_2. The NO gas was passed over the protein solution for 5 min with manual agitation to ensure complete reaction. A change from colorless to green-brown was immediately observed. The NO stream was replaced by an argon stream for 10 min to remove excess NO. Samples for EPR were anaerobically transferred to appropriate cells and frozen in liquid nitrogen approximately 45 min after NO addition.

Addition of NO via NONOates. NONOates are compounds that are stable at high pH, but decompose to NO gas at pH 7 (*29*, *30*). They are useful as a means for delivering precisely known amounts of NO in aqueous solutions. NONOates were stored as concentrated stocks in 10 mM NaOH. The rate of decomposition was determined by introducing a small volume of concentrated NONOate into a 25 mM MOPS (pH 7.0) solution and observing the disappearance of the

NONOate UV absorption in mock reactions. This known rate of decomposition was used to determine how much NO was present in a protein solution at any given time after introduction of the NONOate.

H_{red} samples were prepared and placed in septum-sealed vials both with and without 2 equiv of protein B. A small amount (<1% of sample volume) of concentrated diethylamine−NONOate (Cayman Chemicals) was added, and the reaction was allowed to proceed until the desired amount of NO was generated. Samples were frozen in EPR tubes.

Stopped-Flow Spectrophotometry. Stopped-flow experiments were performed to observe the reaction of H_{red} with nitric oxide both with and without 2 equiv of protein B. This ratio of B to H was chosen for direct comparison with previously reported stopped-flow studies with dioxygen (*6*). Protein samples, typically 50−150 μM in H_{red}, were loaded anaerobically into Hamilton gastight syringes with Luer-lock fittings. Saturated NO solutions were prepared by first saturating 25 mM MOPS (pH 7.0) solutions with argon gas to remove O_2. The solutions were cooled to 4 °C, and NO gas was bubbled through them for 15−30 min, resulting in a solution of approximately 2.9 mM NO. This solution was diluted to the desired NO concentration with anaerobic buffer and transferred to a Hamilton gastight syringe. Both the protein- and gas-containing syringes were used to load the drive syringes of a HiTech SF61 DX2 stopped-flow instrument. Both syringes were allowed to equilibrate in a constant-temperature bath for 15−30 min before data were recorded. Two detection systems were used. A HiTech UV−vis diode array spectrophotometer collected data over a wide range of wavelengths. A photomultiplier tube and monochromator were used to collect data at single wavelengths.

To examine the effects of the methane substrate, the NO-containing buffer was further treated. An anaerobic methane stock solution was prepared by bubbling argon followed by methane through a septum-sealed vial of 25 mM MOPS (pH 7.0). An aliquot of this solution was mixed in a 1:1 ratio with NO-saturated buffer before being loaded into the stopped-flow syringe.

Rapid Freeze-Quench Mössbauer Sample Preparation. All freeze-quench samples were prepared as described in detail elsewhere (*31*). Rapid freeze-quench samples were prepared with an Update Instruments model 705A computer and syringe-ram apparatus. Protein solution concentrations were 1.1 mM in H_{red} before mixing. NO solutions were prepared by purging a 25 mM MOPS buffer sample with argon and allowing it to come to equilibrium in a chamber at a pressure of 1 atm of NO gas at room temperature. The final NO concentration was approximately 1.9 mM. The reactants were loaded into RFQ syringes and allowed to cool to 4 °C in an ice/water bath. The protein and gas solutions were mixed rapidly, allowed to react for various fixed time periods governed by the length of tubing between the mixing chamber and the nozzle, and then sprayed into isopentane at −140 °C. The resulting snow was packed into Delrin Mössbauer sample holders.

Rapid Freeze-Quench EPR Sample Preparation. Rapid freeze-quench samples were prepared by using an Update Instruments model 715 syringe-ram apparatus. Solutions of proteins and NO gas were prepared in a manner similar to that described above for the stopped-flow procedures. H_{red} concentrations were approximately 300 μM before mixing. The reactants were loaded into gastight syringes and cooled to 4 °C. The solutions were mixed rapidly, allowed to react for fixed time periods (28 ms to 60 s) in the aging tubing, and then sprayed into isopentane at approximately −140 °C. The resulting snow was packed into quartz EPR tubes.

EPR Measurements. X-band EPR spectra were measured on a Bruker ESP 300 spectrometer equipped with an Oxford EPR 900 liquid helium cryostat. Spectra were recorded under the following conditions: temperature, 4.2−8.0 K; microwave frequency, 9.41−9.65 GHz; microwave power, 10 μW to 158 mW; modulation frequency, 100 kHz; and modulation amplitude, 6.64 G. Specific conditions are reported for the individual spectra. EPR quantitation was performed by double integration under nonsaturating conditions by using 0.960 mM $CuSO_4$ and 1 M $NaClO_4$ as a standard. Quantitations were corrected for *g*-value anisotropy and spin. EPR power saturation data were collected by measuring signal intensity as a function of the applied microwave power over a range of 4 orders of magnitude.

Mössbauer Measurements. Mössbauer spectra were collected by using either a weak-field spectrometer equipped with a Janis 8DT variable-temperature cryostat or a strong-field spectrometer outfitted with a Janis 12 CNDT/SC SuperVaritemp cryostat encasing an 8 T superconducting magnet. Both spectrometers were operated in a constant acceleration mode in a transmission geometry. The centroid of a room-temperature iron foil spectrum was used as the zero velocity reference point.

Nitrous Oxide Detection by Gas Chromatography. Solutions of H_{red} both with and without 2 equiv of protein B were prepared in 1 mL septum-sealed vials. The concentrations of these samples were ∼300 μM in H_{red}, and the volumes were 300 μL. A saturated 2.9 mM NO buffer sample was prepared at 4 °C as described above. A 100 μL aliquot of the NO buffer was added to the protein sample. At 5 and 30 min intervals after NO addition, 50 μL headspace aliquots were removed and injected onto a Hewlett-Packard 5890 gas chromatograph equipped with a 6 ft packed Haysept column and a thermal conductivity detection system. The column He gas flow rate was 21−23 mL/min at 35 °C. Under these conditions, retention times for various gases were determined to be ∼1.3 min for N_2 and NO and 5.1−5.2 min for N_2O. N_2O standards were prepared by assembling mock reaction vials with BSA at weight per volume concentrations equivalent to that of the hydroxylase in 25 mM MOPS buffer. Known amounts of N_2O were injected into these vials, and they were subjected to the same 5 and 30 min 50 μL headspace analysis as the H_{red}/NO samples. Several N_2O vials were analyzed, and a standard curve was constructed.

RESULTS

Preparation of NO Complexes of H_{red} and H_{red}+2B. Addition of NO gas to samples of H_{red} and H_{red} with 2 equiv of protein B (H_{red}+2B) immediately afforded greenish brown solutions, henceforth designated H_{red}+NO and H_{red}+2B+NO, respectively. The NO addition method was varied and included direct addition of excess NO gas, direct addition of limited quantities of NO gas by a gastight Hamilton syringe, addition of NO via a NONOate precursor, and addition of NO by NO-saturated buffer. No appreciable difference was observed in the resulting optical or EPR

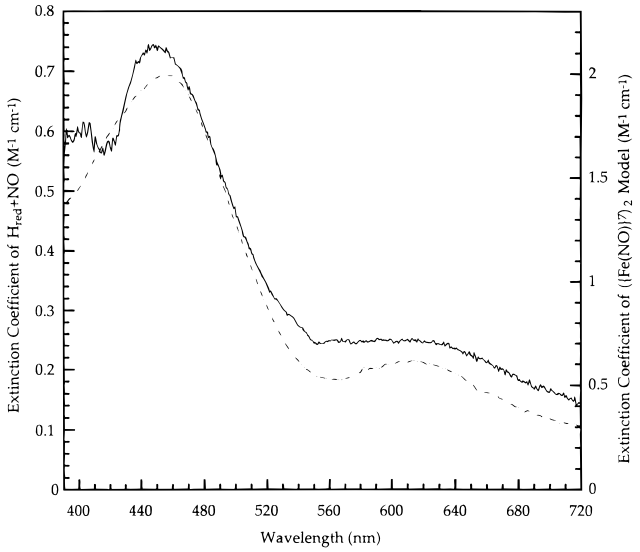

FIGURE 1: Optical spectra of the nitrosyl adduct of the reduced sMMO hydroxylase in 25 mM MOPS (pH 7.0) (solid line) and the dinitrosyl adduct of [Fe_2(μ-XDK)(μ-O_2CPh)($ImH)_2$(O_2CPh)(MeOH)] in THF (dashed line) (*33*).

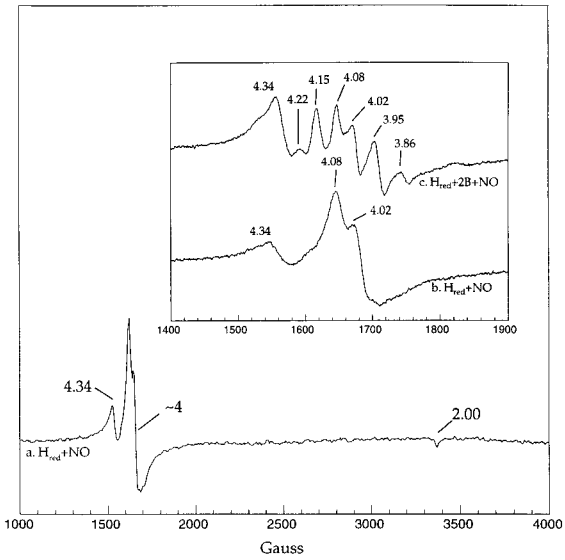

FIGURE 2: EPR spectra of H_{red} (a and b) and H_{red} in the presence of 2 equiv of protein B (c) exposed to NO for 45 min. Spectra were obtained at 4.3−4.8 K, 100 μW, and 9.41 GHz. The buffer was 25 mM MOPS (pH 7.0).

spectral results for samples generated by these different methods.

Optical Absorption Spectra. The optical spectrum of the H_{red}+NO adduct is shown in Figure 1, with maxima at 450 and 620 nm. The extinction coefficient at 450 nm was estimated to be ~740 M^{-1} cm^{-1} assuming that the nitrosyl adducts form 100% of the products. This value should therefore be considered as a lower limit. The spectrum of the H_{red}+2B+NO complex was nearly identical, the only difference being a small decrease in ϵ to approximately ~700 M^{-1} cm^{-1}.

These spectra are quite similar to that of the dinitrosyl adduct of [Fe_2(μ-XDK)(μ-O_2CPh)($ImH)_2$(O_2CPh)(MeOH)] (*32*, *33*), also shown in Figure 1. This compound has a ligand composition nearly identical to that of H_{red} and displays a similar reactivity toward dioxygen. Colored intermediates with characteristic peroxo-to-iron charge transfer bands form rapidly upon reaction with dioxygen. This compound forms a dinitrosyl adduct upon reaction with NO, as established by Mössbauer and EXAFS spectroscopy (*33*).

EPR Analysis of H_{red}+NO and H_{red}+2B+NO Samples. Figure 2 shows the X-band EPR spectra of the H_{red}+NO and H_{red}+2B+NO adducts at 4−5 K. The major signal in the H_{red}+NO spectra has g values of 4.08, 4.02, and 2.00 and arises from an $S = {}^3/_2$ species consistent with mononuclear {Fe(NO)}^{7}. Determination of the spin concentration of this signal from several independent samples showed that it represents 20−30% of the total iron. The half-saturation power ($P_{1/2}$) for this {Fe(NO)}^{7} center was determined to be ~7 mW. The signal splits into at least three species with slightly different rhombicities ($g = 4.08$ and 4.02, $g = 4.15$ and 3.95, and $g = 4.22$ and 3.86) upon addition of protein B. This splitting was observed by addition of protein B either before or after NO exposure. Mononuclear Fe(III) associated with exogenous iron impurities is also present, exhibiting a $g = 4.3$ high-spin ferric signal. Spin quantitation of this signal reveals that it represents 2−6% of total iron in the sample.

Stopped-Flow Analysis of the H_{red}+NO and H_{red}+2B+NO Reaction. Stopped-flow optical spectrophotometry was used to analyze the kinetics of formation and decay of species formed in the reaction of NO with the reduced diiron center of the hydroxylase. As shown in Figure 3, an optical signal with maxima at 450 and 620 nm builds up rapidly upon mixing, maximizing at ~150 ms. After 150 ms, the signal decays slowly until all visible changes stop, approximately 20−30 min after NO addition. At that time, the signal had approximately half of the intensity of its maximum value at 150 ms. The buildup was best fit by a biphasic A → B → C model that, at 4 °C, had the following rate constants: $k_1 = 78 \pm 6$ s^{-1} and $k_2 = 18 \pm 2.7$ s^{-1}. Global analysis of the stopped-flow data revealed that the spectra of species B and C in the two-phase model were nearly identical, the only difference being a 1−2% decrease in the extinction coefficient for B. The decay of the optical signal could not be fit well to any specific model, indicating that it is a complex process comprising several component reactions. First-order fits approximating the decay at 4 °C produced a rate constant of 0.06 ± 0.02 s^{-1}. Variation of the NO concentration over a 10-fold range did not appreciably change the observed rate constants. All stopped-flow experiments subsequently reported here were conducted with at least a 20-fold excess of NO. The temperature dependence of the rate constants for buildup of the optical species was measured. Eyring plots of these data yielded the activation parameters shown in Table 3. A simulation of the time-dependent growth and decay of species formed in the H_{red}+NO reaction, obtained by using the rate constants obtained from stopped-flow data, is presented in Figure 4.

The reaction of NO with the reduced hydroxylase in the presence of 2 equiv of protein B was also examined by stopped-flow spectroscopy. The optical signals detected were essentially identical to those in the H_{red}+NO reactions, the major difference being a small diminution in the observed extinction coefficient as described above. The buildup of this species could, in contrast with the H_{red}+NO reactions, be fit well by a single-exponential buildup. At 4 °C, the rate constant k was determined to be 26 ± 0.8 s^{-1}. The decay, as in the H_{red}+NO case, was too complex to be fit

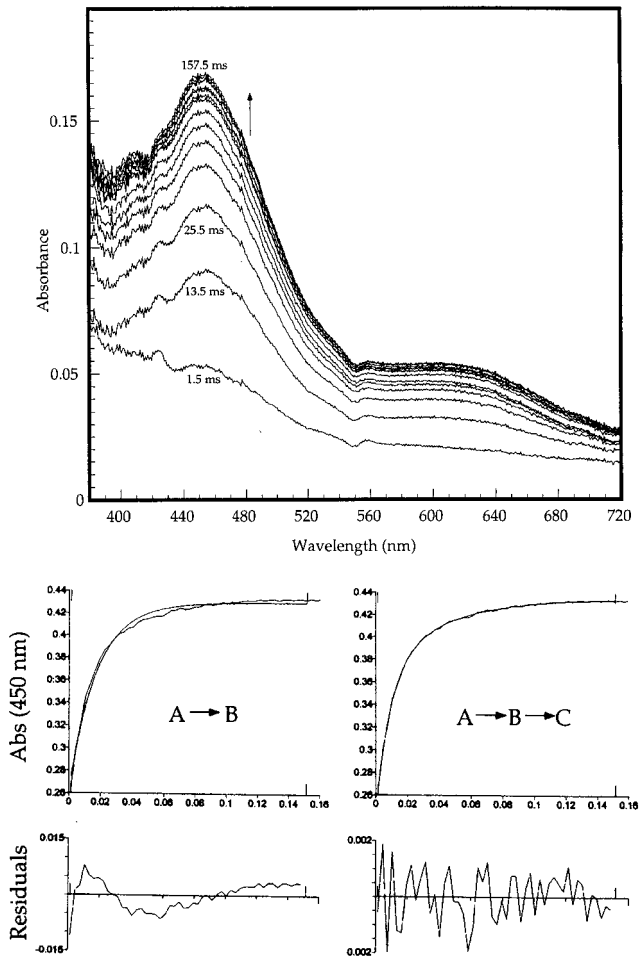

FIGURE 3: (Top) Buildup of the optical species associated with reaction of NO with H_{red} as observed by using stopped-flow spectroscopy at 4 °C. (Bottom) Two comparative fits of the stopped-flow data. The first graph is a fit of the data to an A → B buildup model, and the second is a fit to an A → B → C buildup.

Table 2: Time-Dependent Changes in the Mössbauer Spectra of Rapid Freeze-Quench Time Points of the Reactions of Nitric Oxide with the Reduced sMMO Hydroxylase

species	percentage of species after mixing			Mössbauer properties	
	61 ms	126 ms	440 ms	δ (mm/s)	ΔE_Q (mm/s)
H_{red}	54	57	53	1.30	2.87
H_{ox}	11	10	8	0.57	0.98
$H_{dinitrosyl}$	15	14	10	0.72	1.55
mononuclear $\{Fe(NO)\}_7$	20	19	20	0.7	−1.7
unidentified	–	–	9	0.19	0.63

Table 3: Activation Parameters from Eyring Plots of the Reaction of the Reduced Hydroxylase with Nitric Oxide

reaction	$\Delta H^{\ddagger}$ (kcal mol^{-1})	$\Delta S^{\ddagger}$ (cal mol^{-1} K^{-1})
H_{red}+NO, fast phase	13.5 ± 5.6	−1.1 ± 4.5
H_{red}+NO, slow phase	15.8 ± 1.3	4.3 ± 3.0
H_{red}+2B+NO	7.3 ± 0.8	−24.9 ± 2.4

satisfactorily by a simple model. First-order approximation of the decay yielded a rate of 0.05 ± 0.02 s^{-1}, the same value within error as for the H_{red}+NO reaction. Temperature-dependent studies of this reaction produced the activation parameters listed in Table 3.

The kinetics of the H_{red}+NO and H_{red}+2B+NO reactions were also examined in the presence of methane. The optical bands that appeared were identical to those formed without methane present. The rates for both reactions could be fit well by first-order equations, from which were derived the following rate constants: $k = 34 \pm 2.3$ s^{-1} for H_{red}+NO and $k = 16 \pm 1.2$ s^{-1} for the reaction in the presence of 2 equiv of protein B.

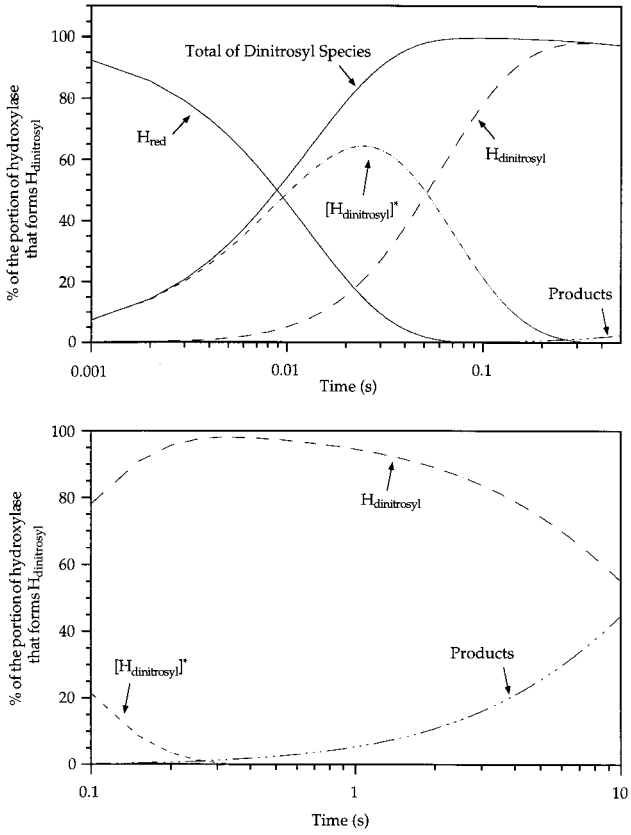

FIGURE 4: Simulation of the $H_{dinitrosyl}$ formation and decay reactions using rate constants derived from stopped-flow data. (Top) Simulation of the first 500 ms of reaction. Also plotted is the total of the two dinitrosyl species, which corresponds to a fit of the stopped-flow optical data. (Bottom) Simulation of the reaction from 100 ms to 10 s.

Rapid Freeze-Quench EPR Characterization of H_{red}+NO Reaction Species. Freeze-quench samples of the H_{red}+NO reaction were collected at 28 ms, 158 ms, 1 s, and 60 s. Spectra taken from those samples are shown in Figure 5. The signal corresponding to the $S = {}^3/_2$ $\{Fe(NO)\}^7$ species can be seen growing in at 28 ms, achieving its maximal value in the 158 ms sample. Fits of these data indicate that the first-order rate constant for the buildup of this signal is 10−20 s^{-1} at 4 °C. Its concentration, 27% of the total amount of iron centers in the sample, does not change within the error limits of the experiment after this time point (see the inset of Figure 5). The signal at $g = 1.97$ is due to free NO in solution, and decreases in intensity during the time course. In the 60 s sample, a signal at $g = 2.04$ has appeared. This signal is most likely due to a small amount of some $S = {}^1/_2$, $Fe(NO)_2$ species. It accounts for <2% of the total iron in the sample.

Mössbauer Characterization of H_{red}+NO Reaction Species. The protein concentration used in these experiments was much higher than that in other H_{red}+NO work, to optimize the signal-to-noise ratio that could be obtained with Mössbauer spectroscopy. A consequence of this limitation is that

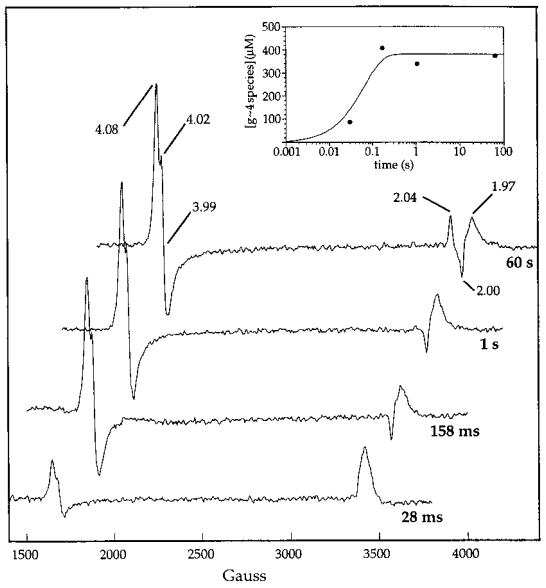

FIGURE 5: Time-dependent RFQ EPR spectra following the reaction of NO with the reduced sMMO hydroxylase at 4 °C. Spectra correspond to reaction times of 28 ms, 158 ms, 1 s, and 60 s. Spectra were obtained at 4.5 K, 100 μW, and 9.41 GHz. The inset is a plot of the concentration of the mononuclear $\{Fe(NO)\}^7$ species as a function of time, with the solid line showing a monophasic fit of the data.

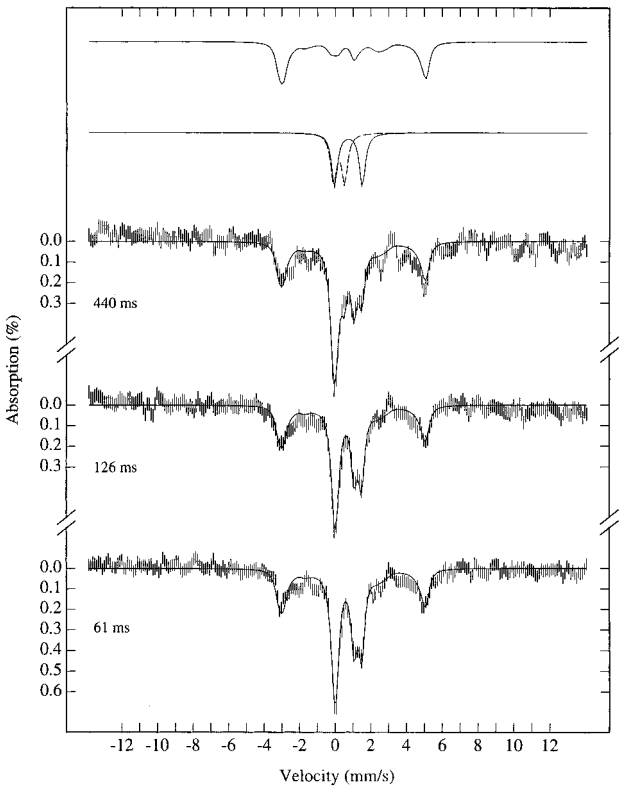

FIGURE 6: Time-dependent Mössbauer spectra following the reaction of H_{red} with NO at 4 °C. (Top spectrum, solid line) Derived spectrum of mononuclear $\{Fe(NO)\}^7$ species. (Middle spectrum, solid line) Derived spectrum of $H_{dinitrosyl}$ species. (Middle spectrum, dotted line) Derived spectrum of "unidentified" species. (Bottom spectra) RFQ Mössbauer time points. The H_{red} Mössbauer spectrum has been subtracted from all time points. The solid line through the data corresponds to simulations using parameters listed in Table 3.

the NO concentration (~1.9 mM) is substoichiometric with respect to the amount of iron (~3.9 mM). As a result, more than 50% of the hydroxylase remains in the reduced state. In addition, the rates of the NO reactions cannot be directly compared with those obtained in the stopped-flow and EPR freeze-quench experiments, because those data were obtained under first-order conditions where NO was in great excess.

Figure 6 shows the Mössbauer spectra of the reaction of H_{red} with NO at three different times after mixing, and Table 2 contains the Mössbauer parameters used for the fits to the data. Reactions were quenched at 61, 126, and 440 ms. The major component of all the spectra is a quadrupole doublet that can be attributed to unreacted H_{red}. An ~10% amount of H_{ox} can be seen in all samples that cannot be reduced, as previously observed for the *M. capsulatus* (Bath) hydroxylase (*6*). These two species can be identified in the spectra according to their previously identified characteristics (*6*, *34*). A paramagnetic species, the spectrum of which is shown as a solid line at the top of Figure 6, corresponding to an $S = {}^3/_2$ mononuclear $\{Fe(NO)\}^7$ complex develops very quickly, reaching its maximal concentration before 61 ms. It does not decay until after 440 ms, in accord with the freeze-quench EPR data. A species exhibiting a quadrupole doublet, shown as a solid line in the middle spectrum of Figure 6, is also present. The Mössbauer parameters of this species ($\delta = 0.72$ mm/s and $\Delta E_Q = 1.55$ mm/s) are also characteristic of $\{Fe(NO)\}^7$ (*22*, *26*). The fact that it exhibits a quadrupole doublet at 4.2 K, however, suggests that the species has integer spin, and spectra recorded at an 8 T applied field revealed it to be diamagnetic ($S = 0$). These spectroscopic properties are indicative of an antiferromagnetically exchange-coupled diiron species containing two $\{Fe(NO)\}^7$ units, similar to the dinitrosyl product observed in the reaction of R2 with NO (*26*). We therefore assign the species as $H_{dinitrosyl}$. It also forms very quickly, consistent with the stopped-flow evidence, and decays to approximately 70% of its maximal value at the 440 ms time point. This rate of decay is slightly faster than that observed in the stopped-flow experiments. Such a difference might arise if the "unidentified" decay product of $H_{dinitrosyl}$ has optical properties similar to those of other iron nitrosyl species, a likely possibility. Thus, the measured decay rate of $H_{dinitrosyl}$, as observed by optical stopped-flow spectroscopy, may be inaccurate because of the buildup of other colored components. The Mössbauer parameters of a decay product from the H_{red}+NO reaction at the 440 ms time point suggest that it may contain an $\{Fe(NO)_2\}$ fragment, although other iron nitrosyl species cannot be ruled out.

The Mössbauer freeze-quench work serves to identify $H_{dinitrosyl}$ species as the EPR-silent reaction component that forms and decays slowly in the stopped-flow experiment (Figure 4). It also supports the rapid freeze-quench EPR data indicating that a mononuclear $\{Fe(NO)\}^7$ species develops very quickly upon reaction of NO with H_{red} and does not decay.

Decay of $H_{dinitrosyl}$ to N_2O. The dinitrosyl adduct of the diiron center in the R2 subunit of ribonucleotide reductase decays slowly with a first-order rate constant of ~0.013 min^{-1} to $R2_{met}$ and N_2O (*26*). To determine whether the sMMO dinitrosyl adduct undergoes similar chemistry, the headspace of a H_{red}+NO sample was analyzed for N_2O by gas chromatography. Samples taken both 5 and 30 min after exposure to NO contained 0.06−0.12 equiv of N_2O per

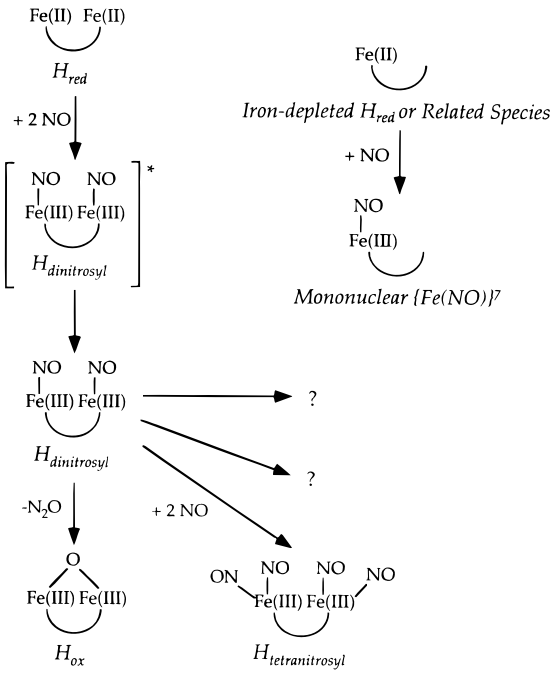

FIGURE 7: Proposed mechanism for the reactions of NO with H_{red}.

hydroxylase diiron center. Similar samples taken of the H_{red}+2B+NO reaction contained 0.10−0.16 equiv of N_2O per hydroxylase diiron center. One possible decay pathway of the $H_{dinitrosyl}$ species is elimination of N_2O, which would likely afford H_{ox} as a byproduct.

DISCUSSION

Reaction of Reduced Hydroxylase with NO To Form a Diiron Dinitrosyl Species. Nitric oxide reacts with the reduced diiron center in the sMMO hydroxylase to afford an EPR-silent product that accounts for most of the iron. We assign this species as $[\{Fe(NO)\}^7]_2$, $H_{dinitrosyl}$. The remainder of the iron is mononuclear (vide infra). These reactions are illustrated in Figure 7. The $H_{dinitrosyl}$ intermediate models H_{peroxo} in the sMMO reaction cycle. Its two $\{Fe(NO)\}^7$ centers antiferromagnetically couple to afford a diamagnetic ground state.

The spectroscopic properties of $H_{dinitrosyl}$ were revealed by stopped-flow, RFQ EPR, and RFQ Mössbauer experiments. When H_{red} is allowed to react with NO, an optical spectrum rapidly grows in, maximizes after approximately 150 ms, and subsequently decays. The optical spectrum closely resembles those of diiron dinitrosyl model complexes (*33*) and a similar dinitrosyl adduct of the ribonucleotide reductase R2 protein (*26*). The optical data are therefore consistent with formation of a diiron dinitrosyl unit, but alone are insufficient to prove that assignment.

Rapid freeze-quench Mössbauer data indicate that only two species containing iron−nitrosyl moieties form within the first 500 ms of reaction. The isomer shifts and quadrupole splitting parameters are consistent with the formation of $H_{dinitrosyl}$ and a mononuclear $\{Fe(NO)\}^7$ center. Rapid freeze-quench EPR and Mössbauer spectroscopy establish that the mononuclear $\{Fe(NO)\}^7$ unit forms in the first 100 ms after NO addition and does not decay even after 60 s of reaction. The RFQ Mössbauer data reveal that the species assigned as $H_{dinitrosyl}$ decays after 150 ms. Because the stopped-flow experiments indicate that the optical bands at 450 and 620 nm bands also decay after 150 ms of reaction, it can be concluded that $H_{dinitrosyl}$ contributes significantly to the observed optical signals.

Although it is possible that the mononuclear $\{Fe(NO)\}^7$ species also absorbs at 450 and 620 nm, its contribution is likely to be minimal. The EPR spectra reveal that most of the iron is diamagnetic; thus, mononuclear species are in a minority. Moreover, both the $H_{dinitrosyl}$ and mononuclear $\{Fe(NO)\}^7$ species appear, from all available data, to build up during the first 200 ms of reaction. If the contribution from a mononuclear $\{Fe(NO)\}^7$ species were similar to that of $H_{dinitrosyl}$, one would expect to be able to distinguish the two formation rates kinetically. Instead, the stopped-flow data could be fit well to simple A → B (H_{red}+2B+NO) and A → B → C (H_{red}+NO) models (vide infra). Fits to A → B, A → C buildup kinetics could not account for the data. It is therefore likely that only one major optical species forms in the H_{red}+NO reaction. Because $H_{dinitrosyl}$ contributes significantly to the optical signals seen in the stopped-flow spectroscopic experiments (vide supra), we conclude that $H_{dinitrosyl}$ is the major component.

A Mononuclear $\{Fe(NO)\}^7$ Minority Species in the H_{red}+NO Reaction. Approximately 20−30% of the protein active sites react with NO to afford a paramagnetic, $S = {}^3/_2$ $\{Fe(NO)\}^7$ unit. This species probably forms in the active site of the hydroxylase, because its EPR characteristics are affected by the presence of protein B (vide infra). We considered the possibility that the $\{Fe(NO)\}^7$ EPR signal might arise by reaction of the active sites to eject one iron atom, leaving the second to react with NO in forming a mononuclear species. Such a mechanism is unlikely, however, since the iron atoms are well-coordinated by protein ligands and are not expected to be extruded from the active site simply by addition of nitric oxide. Moreover, the iron content of the hydroxylase was determined both before and after NO treatment, and no metal was lost as a result of the reaction (data not shown). The sMMO hydroxylase as currently isolated from *M. capsulatus* (Bath) has 3.4−3.7 iron atoms per molecule, fewer than the expected number of 4 if all sites were fully occupied. The absence of one iron atom from 20% of the active sites would amount to a 10% deficiency of total iron, consistent with the measured amount of iron in the protein. We therefore attribute the $\{Fe(NO)\}^7$ signal to mononuclear sites resulting from iron-depleted enzyme. Heterogeneity in the sMMO hydroxylase as isolated has previously been noted in kinetics and spectroscopic experiments (*6*, *35*, *36*).

Effects of Protein B on the Mononuclear $\{Fe(NO)\}^7$ Species. The presence of protein B causes the $S = {}^3/_2$ EPR signal of the $\{Fe(NO)\}^7$ species to split into three signals arising from three species with slightly different rhombicities. This result can be explained by the following model. The species with the least rhombic character ($g = 4.08$ and 4.02) is assigned to hydroxylase having no bound protein B. When protein B binds to this enzyme, the active-site environment is altered, and the $\{Fe(NO)\}^7$ unit assumes a slightly more rhombic coordination environment. This species is assigned to the $g = 4.15$ and 3.95 signal. When a second molecule of protein B is bound, the iron-site rhombicity is shifted even further, resulting in the observation of yet a third signal. Although interesting, this information is of limited value,

for it is impossible to assign specific structures to the EPR-observed species, and it is unlikely that the hydroxylase sites housing the $\{Fe(NO)\}^7$ centers have their native conformation.

Comparison between the Reactions of the sMMO Hydroxylase with NO and O_2. The reaction of reduced hydroxylase with dioxygen in the absence of protein B has not been investigated in detail. Under these conditions, the consumption of electrons and dioxygen is completely uncoupled from substrate hydroxylation (*13*), although the hydroxylase does become oxidized. Intermediates H_{peroxo} and Q do not accumulate. By contrast, the reaction of H_{red} and 2 equiv of protein B with O_2 has been well-characterized (*6*, *7*). The first step is the formation of the H_{peroxo} intermediate, which is most likely a (μ-1,2-peroxo)diiron(III) species. Further reaction produces intermediate Q, which oxidizes substrate. There are clear differences between the reactions with and without protein B.

The reaction of H_{red} with NO to form the H_{peroxo} analogue $H_{dinitrosyl}$, however, occurs whether or not protein B is present. There are two possible models to explain this difference. If the binding of protein B to the hydroxylase modulates the iron−iron distance, in the absence of this component the iron atoms may not have the correct separation to accommodate a peroxide-bridged structure. If dioxygen were to bind under such circumstances, it might be reduced to the superoxo or peroxo (as in hemerythrin) level but not react further without being released from iron. The binding of protein B might bring the iron atoms to the proper distance to support 1,2-peroxo bridge formation. With NO as the reactant, the iron−iron distance should not be an issue, and a dinitrosyl species should form whether or not protein B is present. In the second model, protein B adjusts the relative orientations of the available coordination sites in H_{red}. Without protein B present, the coordination sites may be positioned such that peroxide cannot bridge. Binding of protein B may cause a shift of the ligands such that the available coordination sites are oriented to facilitate formation of a peroxide bridge. Such shifting would not be required for NO binding to the two iron atoms. These two models are not mutually exclusive.

The available crystallographic data for reduced sMMO hydroxylase (*37*) are consistent with aspects of both models, as illustrated in Figure 8. The iron−iron distance in the diiron(II) center is 3.28 Å, shorter than the 4.0 Å distance in a crystallographically characterized (μ-1,2-peroxo)-diiron(III) model complex having the same Mössbauer isomer shift as H_{peroxo} (*8*). Moreover, there are two sites in the reduced diiron center structure that are occupied by very weakly bound water molecules, and are therefore available for exogenous ligand binding. These sites are approximately 80°, or gauche, to one another when viewed down the iron−iron axis, as illustrated in Figure 8. Binding of protein B may shift the coordination environment so as to bring these open coordination sites into a more eclipsed conformation and possibly also to alter the iron−iron distance. In Figure 9, this model is elaborated by hypothesizing that Glu243 undergoes a carboxylate shift, bridging the two iron atoms in a μ-1,2 fashion, as previously hypothesized (*37*). The resulting diiron environment is very much like that in the ribonucleotide reductase $R2_{red}$ structure (*38*), where the available coordination sites are adjacent to one another and where a peroxo intermediate has also been characterized (*39*).

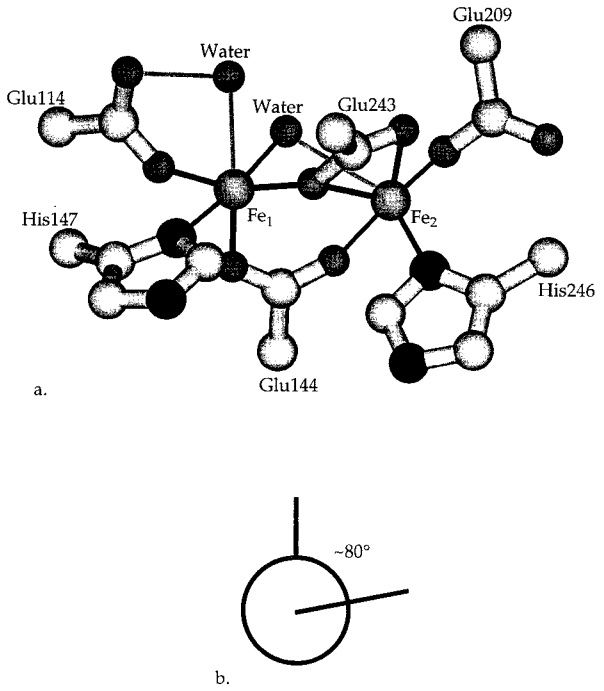

FIGURE 8: Active-site structure of the reduced sMMO hydroxylase. (a) Ligand arrangement around the iron site. Note that the open coordination sites on each iron are occupied by weakly bound water ligands. (b) Newman projection viewed down the Fe−Fe axis in the H_{red} active site. The positions of the open coordination sites are shown. This figure was prepared with MolScript (*47*).

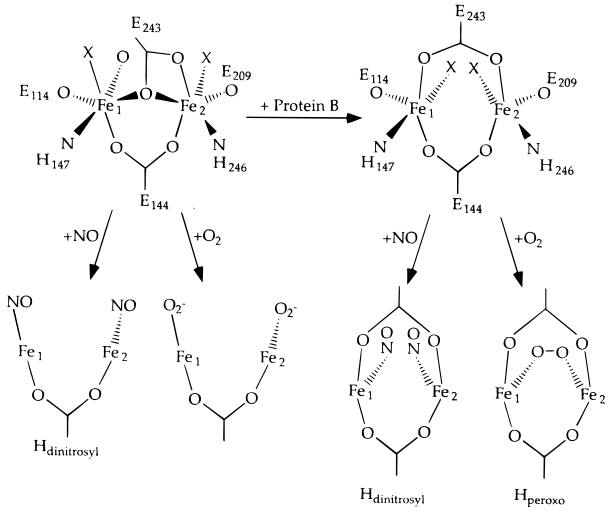

FIGURE 9: Proposal for ligand movements in the active site of the reduced sMMO hydroxylase induced by binding of protein B. The schematic diagram for the H_{red} active site is taken from the crystal structure of the reduced sMMOH and the H_{red}+2B active site from the crystal structure of the reduced R2 subunit.

Details of this model may be altered when information about the structure of the complex between the hydroxylase and protein B becomes available.

Buildup of $H_{dinitrosyl}$. The formation of $H_{dinitrosyl}$ from the reaction of H_{red} with NO in the absence of protein B and methane clearly follows biphasic kinetics. There are several possible interpretations of this result. The first is that the initial intermediate formed is a mononitrosyl species, with an NO molecule bound to one of the iron atoms. Reaction with a second NO would lead to formation of $H_{dinitrosyl}$. This hypothesis is not consistent with the available data, however. Such a mononitrosyl species would be expected to have

spectroscopic properties very similar to those of the hemerythrin nitrosyl adduct (*25*). The ferrous iron and resulting $\{Fe(NO)\}^7$ center would couple antiferromagnetically, forming an $S = {}^1/_2$ paramagnetic species that would be clearly visible by EPR spectroscopy in rapid freeze-quench samples. No such signal was apparent. Moreover, the optical spectrum of the intermediate revealed by global analysis of the stopped-flow data closely resembles that of $H_{dinitrosyl}$. A mononitrosyl species might be expected to have a smaller extinction coefficient.

The preferred explanation is that the initial reaction of the reduced diiron center with NO affords a dinitrosyl intermediate, designated $[H_{dinitrosyl}]^*$, which spontaneously rearranges to the final, $H_{dinitrosyl}$, form. Since the spectra of both species are nearly identical, they most likely have similar structures. It may be that the $[H_{dinitrosyl}]^*$ to $H_{dinitrosyl}$ transition is the result of a shift in the relative positions of the NO ligands, such as that drawn in Figure 9. Another possibility is that the iron ligand environments are largely unchanged, but that formation of the initial $[H_{dinitrosyl}]^*$ species triggers a conformational change in the hydroxylase, producing $H_{dinitrosyl}$, which can be resolved kinetically.

The result that a diiron mononitrosyl intermediate does not accumulate in the reaction of NO with the reduced hydroxylase has implications for the dioxygen reaction. In particular, there appears to be a readily available coordination site on each iron atom in the active site, allowing rapid formation of the diiron dinitrosyl species without buildup of a diiron mononitrosyl intermediate. This result implies that the dioxygen reaction may proceed similarly, with near simultaneous reaction of both oxygen atoms with the two iron atoms, rather than with a hemerythrin-type mechanism, whereby dioxygen binds to just one iron and is reduced to peroxide without or before coordination to the second iron.

When the H_{red}+NO reaction is performed in the presence of protein B, the kinetics of buildup become monophasic; no $[H_{dinitrosyl}]^*$ intermediate is observed. This observation can be interpreted in terms of the ligand rearrangement model (Figure 9). If the $[H_{dinitrosyl}]^*$ to $H_{dinitrosyl}$ transition as observed in reactions without protein B is due to a shift in NO ligands from gauche to eclipsed conformations, the shift to monophasic kinetics upon addition of protein B is a reasonable consequence of that model.

The pseudo-first-order rate constant for reaction of NO with H_{red}+2B to form $H_{dinitrosyl}$ at 4 °C is $\sim 26\ s^{-1}$. This value is nearly identical to the rate constant for reaction of O_2 with H_{red}+2B to form H_{peroxo} at 4 °C ($\sim 25\ s^{-1}$) (*40*). The rate constants for the initial reaction with NO and O_2 with H_{red} alone cannot be compared, since no value is available for the latter reaction. The rate constant for the initial reaction with NO ($\sim 78\ s^{-1}$) is much larger than that with protein B present, however, which suggests that the corresponding reaction with dioxygen would also be much faster.

An investigation of the H_{red}+NO reaction without protein B, but in the presence of methane, revealed monophasic buildup. This kinetic behavior is similar to that observed in the presence of protein B, a result suggesting that protein B and methane gas might be able to modify the sMMO hydroxylase structure in a similar way. For example, it may be that both protein B and methane serve to extrude weakly bound water from the diiron center, clearing the way for dioxygen and nitric oxide exogenous ligand binding. One of the two kinetically observable steps in the H_{red}+NO stopped-flow experiments might therefore be loss of bound water. Addition of methane or protein B would facilitate this reaction, resulting in first-order kinetics. A similar effect is well known in the cytochromes P-450 (*41*), where substrate binding to the protein facilitates loss of a water ligand from the heme cofactor. This explanation is also consistent with the activation parameters determined for the reactions of H_{red}+NO and H_{red}+2B+NO, as reported in Table 3. For the reaction of NO with H_{red} in the presence of protein B, a $\Delta S^{\ddagger}$ value of -24.9 cal mol^{-1} K^{-1} was calculated. This value is consistent with reorganization of the active-site structure in the transition state during the rate-determining step when the first of two NO molecules binds to the diiron center. The corresponding reaction of NO with H_{red} without protein B has a much less negative $\Delta S^{\ddagger}$ value of -1.1 cal mol^{-1} K^{-1}. This value reflects a compensating entropic gain in the transition state during the $H_{dinitrosyl}$ formation, such as loss of water. These results support the hypothesis that protein B serves to organize the diiron cluster for optimal reaction with dioxygen, as shown in Figure 9. The substrate methane appears to share aspects of this organizational capacity.

Decay of $H_{dinitrosyl}$. The decay of the dinitrosyl species is complex, and stopped-flow data for this process could not be fit well to any single model. The final mixture of products, as observed by Mössbauer spectroscopy, is heterogeneous (data not shown). In one decay pathway, nitrous oxide is eliminated from $H_{dinitrosyl}$ to afford H_{ox}. This reaction is supported by gas chromatographic detection of N_2O in the headspace above the reaction mixture. The ability of protein B to increase the amount of N_2O formed is consistent with the hypothesis that, in $H_{dinitrosyl}$, the two NO molecules are oriented in positions unfavorable for N−N bond formation. Addition of protein B could reposition the two NO-coordinated molecules toward one another, as depicted in Figure 9, to promote ligand migration and subsequent N−N bond formation. The coupling of two metal-bound NO molecules to form N_2O is well precedented in the literature. The dinitrosyl adduct of the ribonucleotide reductase R2 subunit apparently reacts in this manner (vide supra) (*26*). N_2O formation has also been observed in reactions of NO with dicopper(I) complexes (*42*).

A second decay pathway is suggested by the presence of the "unidentified" species in the Mössbauer spectra of H_{red}+NO reaction mixtures. A product with a low isomer shift appears following decay of $H_{dinitrosyl}$ in the freeze-quench Mössbauer data. This product is diamagnetic, has Mössbauer properties consistent with a high-valent Fe(IV) species, and may contain the $Fe(NO)_2$ fragment. The data are consistent with an active site having two such $\{Fe(NO)_2\}$ centers, antiferromagnetically coupled. Formation of such a species might result from further reaction of NO with the diiron center, displacing water or protein side chain ligands. We do not exclude other assignments, however.

Comparison with the NO Reactions of the Reduced Ribonucleotide Reductase R2 Subunit and Hemerythrin. There are many similarities between the reactions of the reduced sMMO hydroxylase and $R2_{red}$ with NO. The major products formed by each enzyme are $[\{Fe(NO)\}^7]_2$ dinitrosyl species that model aspects of peroxo intermediates in the two systems. These dinitrosyl intermediates are metastable. In the R2 system, decay is slow and apparently consists only of coupling to afford $R2_{met}$ and N_2O. The $H_{dinitrosyl}$ adduct decays more rapidly, forming a more complex mixture of

products. A coupling pathway to form N_2O is apparently present, but does not account for all of the $H_{dinitrosyl}$ decay.

The minor products formed in the reactions of NO with $R2_{red}$ and H_{red} are also similar and include mononuclear $\{Fe(NO)\}^7$ centers and unidentified diamagnetic species having Mössbauer parameters consistent with $[\{Fe(NO)_2\}_2]$. This species appears to be a byproduct of $H_{dinitrosyl}$ decay in the sMMO system. The similarities emphasize the close relationship between the structures and functions of these two enzymes, which is to perform chemistry by using dioxygen as a reactant. The NO chemistry contrasts with that of hemerythrin, which forms a relatively homogeneous and stable NO adduct. The function of hemerythrin is to bind dioxygen reversibly, which is consistent with its reaction with NO.

The results presented here have been useful in suggesting specific roles for the action of protein B in the sMMO system. Examination of the NO chemistry of related proteins, including stearoyl Δ-9 desaturase (*43*, *44*), toluene 4-monooxygenase (*45*), and phenol hydroxylase (*46*), would be helpful in elucidating the similarities and differences in the reactivities of these related proteins.

ACKNOWLEDGMENT

We thank Professor J. Stubbe and Dr. P. Riggs-Gelasco for use of the Update Model 715 freeze-quench apparatus, Professor B. M. Hoffman for helpful conversations regarding EPR spectroscopy, and Drs. A. L. Feig, M. Bautista, T. J. Mizoguchi, and A. M. Valentine for valuable discussions.

REFERENCES

1. Valentine, A. M., and Lippard, S. J. (1997) *J. Chem. Soc., Dalton Trans. 21*, 3925−3931.
2. Kurtz, D. M., Jr. (1997) *JBIC, J. Biol. Inorg. Chem. 2*, 159−167.
3. Wallar, B. J., and Lipscomb, J. D. (1996) *Chem. Rev. 96*, 2625−2657.
4. Liu, K. E., and Lippard, S. J. (1995) in *Advances in Inorganic Chemistry* (Sykes, A. G., Ed.) pp 263−289, Academic Press, San Diego, CA.
5. Lipscomb, J. D. (1994) *Annu. Rev. Microbiol. 48*, 371−399.
6. Liu, K. E., Valentine, A. M., Wang, D., Huynh, B. H., Edmondson, D. E., Salifoglou, A., and Lippard, S. J. (1995) *J. Am. Chem. Soc. 117*, 10174−10185.
7. Lee, S.-K., Nesheim, J. C., and Lipscomb, J. D. (1993) *J. Biol. Chem. 268*, 21569−21577.
8. Kim, K., and Lippard, S. J. (1996) *J. Am. Chem. Soc. 118*, 4914−4915.
9. Dong, Y., Yan, S., Young, V. G., Jr., and Que, L., Jr. (1996) *Angew. Chem., Int. Ed. 35*, 618−620.
10. Ookubo, T., Sugimoto, H., Nagayama, T., Masuda, H., Sato, T., Tanaka, K., Maeda, Y., Okawa, H., Hayashi, Y., Uehara, A., and Suzuki, M. (1996) *J. Am. Chem. Soc. 118*, 701−702.
11. Shu, L., Nesheim, J. C., Kauffmann, K., Münck, E., Lipscomb, J. D., and Que, L., Jr. (1997) *Science 275*, 515−517.
12. Green, J., and Dalton, H. (1985) *J. Biol. Chem. 260*, 15795−15801.
13. Gassner, G. T., and Lippard, S. J. (1999) *Biochemistry* (to be submitted for publication).
14. Hendrich, M. P., Münck, E., Fox, B. G., and Lipscomb, J. D. (1990) *J. Am. Chem. Soc. 112*, 5861−5865.
15. Pulver, S., Froland, W. A., Fox, B. G., Lipscomb, J. D., and Solomon, E. I. (1993) *J. Am. Chem. Soc. 115*, 12409−12422.
16. Pulver, S. C., Froland, W. A., Lipscomb, J. D., and Solomon, E. I. (1997) *J. Am. Chem. Soc. 119*, 387−395.
17. Richter-Addo, G. B., and Legzdins, P. (1992) in *Metal Nitrosyls*, Oxford Univeristy Press, New York.
18. Zhang, Y., Pavlosky, M. A., Brown, C. A., Westre, T. E., Hedman, B., Hodgson, K. O., and Solomon, E. I. (1992) *J. Am. Chem. Soc. 114*, 9189−9191.
19. Brown, C. A., Pavlosky, M. A., Westre, T. E., Zhang, Y., Hedman, B., Hodgson, K. O., and Solomon, E. I. (1995) *J. Am. Chem. Soc. 117*, 715−732.
20. Enemark, J. H., and Feltham, R. D. (1974) *Coord. Chem. Rev. 13*, 339−406.
21. Nelson, M. J. (1987) *J. Biol. Chem. 262*, 12137−12142.
22. Arciero, D. M., Lipscomb, J. D., Huynh, B. H., Kent, T. A., and Münck, E. (1983) *J. Biol. Chem. 258*, 14981−14991.
23. Arciero, D. M., Orville, A. M., and Lipscomb, J. D. (1985) *J. Biol. Chem. 260*, 14035−14044.
24. Nocek, J. M., Kurtz, D. M., Jr., Sage, J. T., Debrunner, P. G., Maroney, M. J., and Que, L., Jr. (1985) *J. Am. Chem. Soc. 107*, 3382−3384.
25. Nocek, J. M., Kurtz, D. M., Jr., Sage, J. T., Xia, Y.-M., Debrunner, P., Shiemke, A. K., Sanders-Loehr, J., and Loehr, T. M. (1988) *Biochemistry 27*, 1014−1024.
26. Haskin, C. J., Ravi, N., Lynch, J. B., Münck, E., and Que, L., Jr. (1995) *Biochemistry 34*, 11090−11098.
27. Willems, J.-P., Valentine, A. M., Gurbiel, R., Lippard, S. J., and Hoffman, B. M. (1998) *J. Am. Chem. Soc. 120*, 9410−9416.
28. Liu, K. E., Johnson, C. C., Newcomb, M., and Lippard, S. J. (1993) *J. Am. Chem. Soc. 115*, 939−947.
29. Maragos, C. M., Morley, D., Wink, D. A., Dunams, T. M., Saavedra, J. E., Hoffman, A., Bove, A. A., Issac, L., Hrabie, J. A., and Keefer, L. K. (1991) *J. Med. Chem. 34*, 3242−3247.
30. Morley, D., and Keefer, L. K. (1993) *J. Cardiovasc. Pharmacol. 22*, S3−S9.
31. Ravi, N., Bollinger, J. M., Jr., Huynh, B. H., Edmundson, D., and Stubbe, J. (1994) *J. Am. Chem. Soc. 116*, 8007−8014.
32. Herold, S., and Lippard, S. J. (1997) *J. Am. Chem. Soc. 119*, 145−156.
33. Mizoguchi, T. J., DuBois, J. L., Bautista, M. T., Hedman, B., Hodgson, K. O., and Lippard, S. J. (1999) *Inorg. Chem.* (to be submitted for publication).
34. DeWitt, J. G., Bentsen, J. G., Rosenzweig, A. C., Hedman, B., Green, J., Pilkington, S., Papaefthymiou, G. C., Dalton, H., Hodgson, K. O., and Lippard, S. J. (1991) *J. Am. Chem. Soc. 113*, 9219−9235.
35. Shu, L., Liu, Y., Lipscomb, J. D., and Que, L., Jr. (1996) *JBIC, J. Biol. Inorg. Chem. 1*, 297−304.
36. Davydov, R., Valentine, A. M., Komar-Panicucci, S., Hoffman, B. M., and Lippard, S. J. (1999) *Biochemistry* (in press).
37. Rosenzweig, A. C., Nordlund, P., Takahara, P. M., Frederick, C. A., and Lippard, S. J. (1995) *Chem. Biol. 2*, 409−418.
38. Åberg, A. (1993) Ph.D. Dissertation, Stockholm University, Stockholm, Sweden.
39. Bollinger, J. M., Jr., Krebs, C., Vicol, A., Chen, S., Ley, B. A., Edmondson, D. E., and Huynh, B. H. (1998) *J. Am. Chem. Soc. 120*, 1094−1095.
40. Valentine, A. M., Stahl, S. S., and Lippard, S. J. (1999) *J. Am. Chem. Soc.* (in press).
41. Sono, M., Roach, M. P., Coulter, E. D., and Dawson, J. H. (1996) *Chem. Rev. 96*, 2841−2887.
42. Paul, P. P., and Karlin, K. D. (1991) *J. Am. Chem. Soc. 113*, 6331−6332.
43. Fox, B. G., Shanklin, J., Somerville, C., and Münck, E. (1993) *Proc. Natl. Acad. Sci. U.S.A. 90*, 2486-2490.
44. Fox, B. G., Shanklin, J., Ai, J., Loehr, T. M., and Sanders-Loehr, J. (1994) *Biochemistry 33*, 12776−12786.
45. Pikus, J. D., Studts, J. M., Achim, C., Kauffmann, K. E., Münck, E., Steffan, R. J., McClay, K., and Fox, B. G. (1996) *Biochemistry 35*, 9106−9119.
46. Nordlund, I., Powlowski, J., and Shingler, V. (1990) *J. Bacteriol. 172*, 6826−6833.
47. Kraulis, P. J. (1991) *J. Appl. Crystallogr. 24*, 946−950.
48. Feig, A. L., Bautista, M. T., and Lippard, S. J. (1996) *Inorg. Chem. 35*, 6892−6898.

BI9823378